

Communication

# The ZrO<sub>2</sub> Formation in ZrB<sub>2</sub>/SiC Composite Irradiated by Laser

Ling Liu <sup>1,2,\*</sup>, Zhuang Ma <sup>1,2</sup>, Zhenyu Yan <sup>1,2</sup>, Shizhen Zhu <sup>1,2</sup> and Lihong Gao <sup>1,2</sup>

Received: 3 November 2015; Accepted: 3 December 2015; Published: 14 December 2015

Academic Editor: Luciano Feo

<sup>1</sup> School of Materials Science and Engineering, Beijing Institute of Technology, Beijing 100081, China; hstrong929@bit.edu.cn (Z.M.); yanzhenyu@bit.edu.cn (Z.Y.); zhusz@bit.edu.cn (S.Z.); gaolihong@bit.edu.cn (L.G.)

<sup>2</sup> National Key Laboratory of Science and Technology on Materials under Shock and Impact, Beijing 100081, China

\* Correspondence: richard@bit.edu.cn; Tel.: +86-10-6891-1144 (ext. 865); Fax: +86-10-6891-1144 (ext. 869)

**Abstract:** In order to clearly understand the details of ZrO<sub>2</sub> formation during ablation, high intensity continuous laser was chosen to irradiate ZrB<sub>2</sub>/SiC. The results reveal that there are two different modes of ZrO<sub>2</sub> formation depending on whether liquid SiO<sub>2</sub> is present. When liquid SiO<sub>2</sub> is present, ZrO<sub>2</sub> generated by the oxidation of ZrB<sub>2</sub> is firstly dissolved into SiO<sub>2</sub>. Then, ZrO<sub>2</sub> will precipitate again, the temperature will decrease and the SiO<sub>2</sub> will evaporate. Otherwise, the ZrB<sub>2</sub> will be oxidized to ZrO<sub>2</sub> directly.

**Keywords:** ZrB<sub>2</sub>/SiC; laser irradiation; ZrO<sub>2</sub> formation

## 1. Introduction

Ultra high temperature ceramics (UHTCs) refer to a class of refractory materials with melting temperatures in excess of 3000 °C, such as diborides and carbides of transition metals [1,2]. As a member of UHTCs, zirconium diboride (ZrB<sub>2</sub>) has been widely attractive for decades. Because of its excellent properties, such as high melting temperature, high thermal conduction, excellent mechanical properties, *etc.*, ZrB<sub>2</sub> can be operated as leading edges in hypersonic vehicles.

According to previous research, ZrB<sub>2</sub>/SiC exhibited excellent ablation resistance against oxyacetylene torch, arc jet or plasma arc [3–5]. No obvious mass loss or macroscopic damage appears. Some products, like SiO<sub>2</sub> and ZrO<sub>2</sub>, can be detected on a microscopic scale, and have been proved to be helpful to improve ZrB<sub>2</sub>/SiC's ablation resistance [6,7]. However, the upper surface of the sample is wholly heated by the above ablation method, and we could only obtain the information of phase and microstructure until the ablated sample cools completely. Longer cooling time contributes to ablation transformation. So some important characterized information has been concealed or disappeared during the cooling process. Researchers only observed that the ablated layer of ZrB<sub>2</sub>/SiC was composed by ZrO<sub>2</sub> skeleton and liquid SiO<sub>2</sub> [8,9]. The real process and details of the formation of oxidation product, especially ZrO<sub>2</sub>, are still unknown.

If the information of phase and microstructure under high temperature can be preserved by fast cooling, the real transformation will be easily observed at room temperature. Because of this theory, the high intensity laser ablation method with rapid heating rate was utilized. The local temperature of ZrB<sub>2</sub>/SiC at the spot center can reach thousands of degrees instantaneously at the beginning of laser irradiating. When laser loading stops, the sample can cool down rapidly to room temperature (which is similar to quenching), since the heating area is very small and the emissivity and conductivity of ZrB<sub>2</sub>/SiC are very high [10,11].

In this paper,  $ZrB_2/20 \text{ vol } \% \text{ SiC}$  composite (donated as ZS hereafter) was prepared and irradiated by high intensity continuous laser. The phase and microstructure evolution of  $ZrB_2/\text{SiC}$  was investigated.

## 2. Results and Discussion

Figure 1 shows the polished surface microstructure of the as-sintered material.  $ZrB_2$  with grain size of about  $5 \mu\text{m}$  is present as a grey matrix, while the dark SiC homogeneously distributes in the matrix.

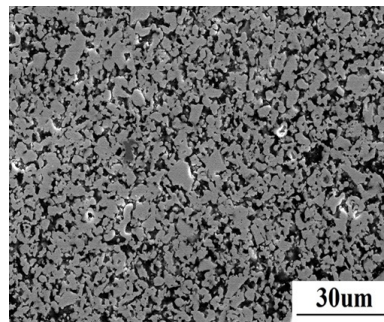


Figure 1. The microstructure of as-sintered  $ZrB_2/\text{SiC}$  composite.

The X-ray diffraction (XRD) result of the  $ZrB_2/\text{SiC}$  surface after laser ablation for 20 s is shown in Figure 2. According to the XRD, m- $ZrO_2$  and  $ZrB_2$  are the major phases on the surface. It reveals that some  $ZrB_2$  are oxidized into  $ZrO_2$  while parts of  $ZrB_2$  are not oxidized at all. No peaks of  $SiO_2$  can be observed on the spectrum, because  $SiO_2$  is amorphous on the surface. However, small amounts of  $ZrSiO_4$  are detected, as shown in the spectrum. This proves that  $SiO_2$  forms, and that parts of  $ZrO_2$  dissolve into  $SiO_2$  to form  $ZrSiO_4$ .

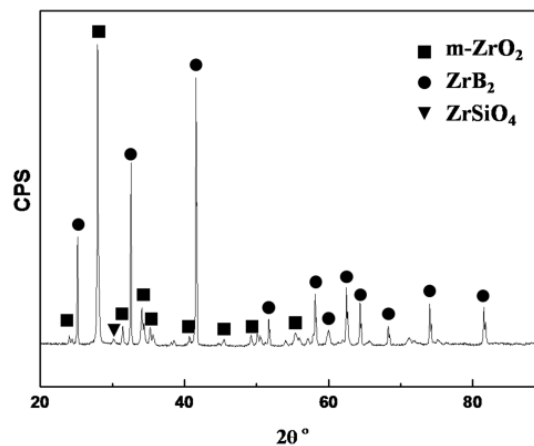
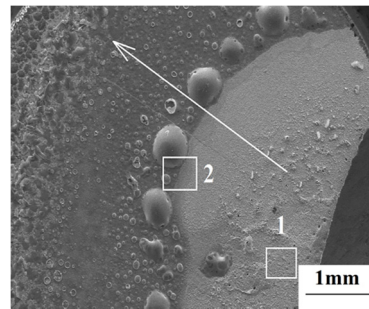


Figure 2. X-ray diffraction (XRD) of the sample surface after ablation for 20 s.

The surface macrostructure of  $ZrB_2/\text{SiC}$  after laser ablation for 20 s is shown in Figure 3. Since the local heating of the laser induces extremely high temperature at the spot center, a great temperature gradient is generated along the radial direction, shown by the arrow in Figure 3. Significant differences in ablation behavior between area 1 and area 2 were detected.



**Figure 3.** The surface macrostructure of the sample after ablation for 20 s.

The surface morphology of area 1 after laser ablation is shown in Figure 4. From Figure 4a, the surface performs a porous structure. The energy dispersive spectroscopy (EDS) result reveals that only  $\text{ZrO}_2$  exists on the surface; neither  $\text{ZrB}_2$  nor  $\text{SiC}$  can be detected. A typical flushing morphology is clearly shown as Figure 4b. It should be attributed to the liquid splashing and the following rapid solidification. This means that the oxidized  $\text{ZrO}_2$  in this region has been totally melted during laser ablation. Meanwhile,  $\text{SiC}$  is totally decomposed because the temperature here is higher than its decomposition point of  $2300\text{ }^\circ\text{C}$ .

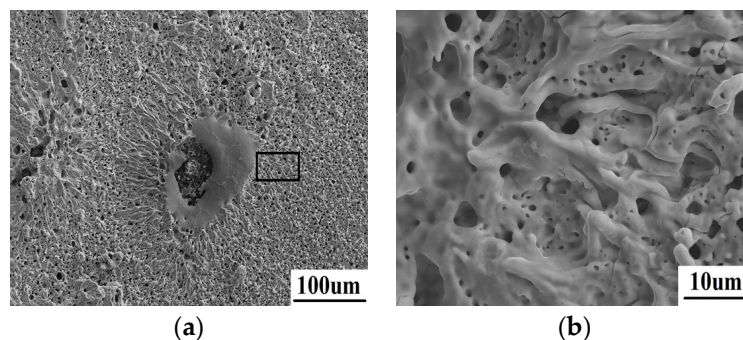


**Figure 4.** The microscopic morphology of area 1 (a) with a typical flushing morphology (b).

The different microstructure in area 2 is shown in Figure 5. According to Figure 5a, lots of white or dark grey particles implant in amorphous substance. Based on the EDS result as shown in Table 1, the particles are  $\text{ZrO}_2$  while the amorphous substance is  $\text{SiO}_2$ . This also can be confirmed by the XRD result shown in Figure 2. The region shown in Figure 5b is farther from the spot center than the region shown in Figure 5c. As can be seen in Figure 5b, very fine sub-micron  $\text{ZrO}_2$  distributes evenly in amorphous  $\text{SiO}_2$ . With the temperature increases from left to right in Figure 5b, amorphous  $\text{SiO}_2$  reduces gradually, while the quantity and size of  $\text{ZrO}_2$  particles increase gradually. In Figure 5c, amorphous  $\text{SiO}_2$  is much lower, even almost disappearing at the right side, which results from the evaporation of  $\text{SiO}_2$ . Moreover,  $\text{ZrO}_2$  grains close to the spot center grow gradually, and can even be seen to sinter obviously.

**Table 1.** The energy dispersive spectroscopy (EDS) results of area B and C in Figure 2.

Elements	Area B		Area C	
	Weight Ratio %	Atomic Ratio %	Weight Ratio %	Atomic Ratio %
O K	36.32	67.85	26.52	66.30
Si K	15.32	16.31	1.51	2.15
Zr L	48.36	15.85	71.97	31.55

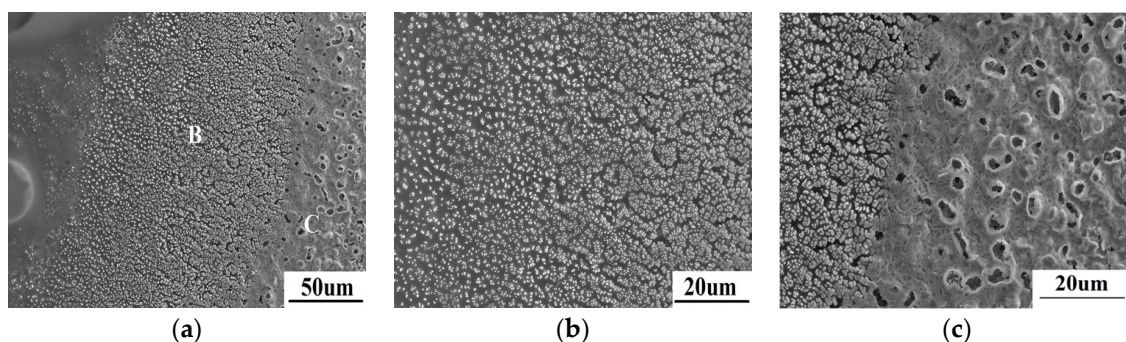


**Figure 5.** The microscopic morphology of area 2 (a) and the further amplified morphology of region B (b) and C (c).

According to the equilibrium phase diagram of  $ZrO_2$ - $SiO_2$  shown as Figure 6 [12], the melting temperature ( $2700\text{ }^\circ\text{C}$ ) of  $ZrO_2$  can be decreased by liquid  $SiO_2$ , while  $ZrO_2$  has high solubility, about 43.3% in  $SiO_2$  at  $2235\text{ }^\circ\text{C}$ . With increasing temperature, the solubility of  $ZrO_2$  will increase gradually. When laser begins to irradiate on the material, the surface temperature soars up rapidly. A large number of  $ZrB_2$  are oxidized into  $ZrO_2$  between  $600\text{--}700\text{ }^\circ\text{C}$ . Meanwhile,  $SiC$  transforms into  $SiO_2$  at  $1200\text{ }^\circ\text{C}$ , and  $SiO_2$  exhibits as a liquid above  $1400\text{ }^\circ\text{C}$ . When the temperature approaches  $1687\text{ }^\circ\text{C}$ , the oxidized  $ZrO_2$  begins to dissolve into  $SiO_2$ .  $SiO_2$  is unstable when the temperature is higher than  $1800\text{ }^\circ\text{C}$  [13]. The evaporation of  $SiO_2$  at high temperature makes the  $ZrO_2$  solubility decrease, so the extremely fine  $ZrO_2$  grains precipitate. With the evaporation proceeding, the solubility of  $ZrO_2$  dissolved into  $SiO_2$  significantly decreases. A lot of  $ZrO_2$  will precipitate from liquid  $SiO_2$  to form the morphology shown in Figure 5b. As precipitated  $ZrO_2$  is still subject to intense high temperature, fine  $ZrO_2$  grains with strong activity gradually grow up and sinter together for a short time to form the morphology as shown in Figure 5c. Therefore, the processing of  $ZrO_2$  dissolution and precipitation is the main transformation mechanism during ablation when liquid  $SiO_2$  is present.

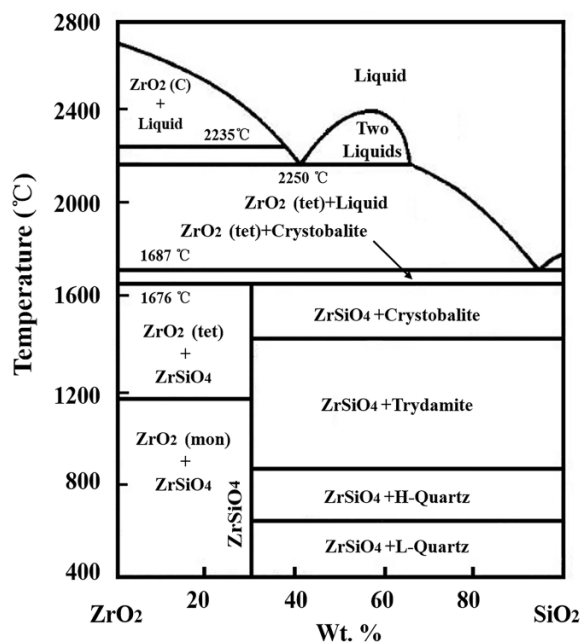


**Figure 6.** Thermal equilibrium phase diagram of  $SiO_2$ - $ZrO_2$ .

The surface microstructure of  $ZrB_2/SiC$  at the edge is shown in Figure 7. The temperature is lower than  $1200\text{ }^\circ\text{C}$  in this region away from the spot center.  $SiC$  oxidation and liquid  $SiO_2$  are

not observed on the surface. The morphology of  $ZrB_2$  has changed because of oxidation. A lot of nano-crystals closely pack on the surface. This is proved to be  $ZrO_2$  according to the EDS result. This indicates that  $ZrB_2$  is directly oxidized into nano- $ZrO_2$ . The results reveal that there is another formation mechanism of  $ZrO_2$  during ablation when liquid  $SiO_2$  is absent.

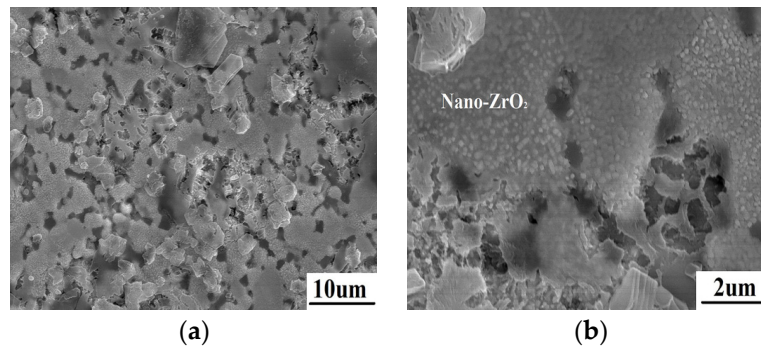


**Figure 7.** The morphology of  $ZrB_2/SiC$  at the edge after ablation (a) with nano  $ZrO_2$  crystals packing on the surface (b).

### 3. Experimental Section

The ZS composite was prepared using commercial powders listed as follows:  $ZrB_2$  (Alfa Aesar Ward Hill, MA, USA, 99.0%, particlesize  $\sim 50 \mu m$ );  $SiC$  (Alfa Aesar, 99.5%, particlesize  $1\text{--}2 \mu m$ ). The raw powders were accurately weighted by volume ratio of 4:1 and milled for 6 h in ethanol using zirconia milling media. The mixture powders were sintered by spark plasma sintering technology (SPS, DR. SINTER type 3.20, Fuji Electronic Industrial Co. Ltd., Kanagawa, Japan) at  $1750 \text{ }^\circ C$  for 5 min with a rate of  $200 \text{ }^\circ C/min$ . An axial pressure of 50 MPa was applied during the whole process.

The laser irradiation experiment in this paper was carried out by using ytterbium laser system (YLS-2000) (IPG Photonics Co. Ltd., Pittsfield, MA, USA), with 1070 nm wave-length in atmospheric environment. The spot size of the Gaussian laser was set as about 10 mm. The power density at the spot center reached  $20 \text{ MW}/m^2$  in Gaussian laser, and the duration time was 20 s. The dimensions of the ablation specimen were  $\Phi 25 \text{ mm} \times 3 \text{ mm}$ .

The phase of the sample surface after ablation was detected by X-ray diffraction (XRD, X'pert PRO MPD, PANalytical B.V. Co. Ltd., Amsterdam, The Netherlands,  $Cu \text{ K}\alpha$ ). The surface microstructures of the sample before and after ablation were examined by scanning electron microscope (SEM, Philips S-4800, Hitachi Ltd., Yokohama, Japan). The composition of the sample was identified by energy dispersive spectroscopy (EDS, Oxford Instruments Co. Ltd., Oxfordshire, UK).

### 4. Conclusions

The  $ZrO_2$  formation in  $ZrB_2/SiC$  composite during ablation was investigated in this paper. A characterized phenomenon at elevated temperature is preserved by using high intensity continuous laser with the rapid heating rate to irradiate. Two mechanisms of the  $ZrO_2$  formation are directly obtained, depending on whether liquid  $SiO_2$  is present. When liquid  $SiO_2$  is present, oxidized  $ZrO_2$  firstly dissolves into  $SiO_2$ . Fine  $ZrO_2$  grains precipitate with the evaporation of liquid  $SiO_2$ , and then grow, and even sinter together. Otherwise, the  $ZrB_2$  will be oxidized into  $ZrO_2$  directly.

**Acknowledgments:** This work was financially supported by the National Natural Science Foundation of China (No. 51102016) and Program for New Century Excellent Talents in University (NCET-11-0788).

**Author Contributions:** Ling Liu discussed the experiment and wrote the manuscript. Zhuang Ma and Shizhen Zhu conceived and designed the experiments. Zhenyu Yan and Lihong Gao performed the experiments and analyzed the data.

**Conflicts of Interest:** The authors declare no conflict of interest.

## References

1. Savino, R.; Fumo, M.D.; Paterna, D. Aerothermodynamic study of UHTC-based thermal protection systems. *Aerosp. Sci. Technol.* **2005**, *9*, 151–160. [[CrossRef](#)]
2. Squire, T.H.; Marschall, J. Material property requirements for analysis and design of UHTC components in hypersonic applications. *J. Eur. Ceram. Soc.* **2010**, *30*, 2239–2251. [[CrossRef](#)]
3. Jin, X.X.; He, R.J.; Zhang, X.H.; Hu, P. Ablation behavior of ZrB<sub>2</sub>-SiC sharp leading edges. *J. Alloy. Compd.* **2013**, *566*, 125–130. [[CrossRef](#)]
4. Wang, X.G.; Liu, J.; Peng, L.M. ZrB<sub>2</sub>-SiC composite parts in oxyacetylenic torch tests: Experimental and computational assessment of chemical, thermal and mechanical behavior. *Mater. Sci. Eng. A* **2011**, *528*, 6896–6906. [[CrossRef](#)]
5. Frederic, M.; Raffaele, S.; Stefano, F.M.; Andrea, M. Plasma wind tunnel testing of ultra high temperature ZrB<sub>2</sub>-SiC composites under hypersonic re-entry conditions. *J. Eur. Ceram. Soc.* **2009**, *30*, 2313–2321.
6. Fahrenholtz, W.G.; Hilmas, G.E.; Chamberlain, A.L.; Zimmermann, J.W. Processing and characterization of ZrB<sub>2</sub>-based ultra-high temperature monolithic and fibrous monolithic ceramics. *J. Mater. Sci.* **2004**, *39*, 5951–5957. [[CrossRef](#)]
7. Zhang, X.H.; Hu, P.; Han, J.C. Structure evolution of ZrB<sub>2</sub>-SiC during the oxidation in air. *J. Mater. Res.* **2008**, *23*, 1961–1972. [[CrossRef](#)]
8. Rezaie, A.; Fahrenholtz, W.G.; Hilmas, G.E. Evolution of structure during the oxidation of zirconium diboride-silicon carbide in air up to 1500 °C. *J. Eur. Ceram. Soc.* **2007**, *27*, 2495–2501. [[CrossRef](#)]
9. Carney, C.M. Oxidation resistance of hafnium diboride-silicon carbide from 1400 to 2000 °C. *J. Mater. Sci.* **2009**, *44*, 5673–5681. [[CrossRef](#)]
10. Meng, S.H.; Chen, H.B.; Hu, J.H.; Wang, Z.W. Radiative properties characterization of ZrB<sub>2</sub>-SiC-based ultrahigh temperature ceramic at high temperature. *Mater. Design.* **2011**, *32*, 377–381. [[CrossRef](#)]
11. Fahrenholtz, W.G.; Hilmas, G.E. Refractory diborides of zirconium and hafnium. *J. Am. Ceram. Soc.* **2007**, *90*, 1347–1364. [[CrossRef](#)]
12. Buttermann, W.C.; Foster, W.R. Zircon stability and the ZrO<sub>2</sub>-SiO<sub>2</sub> phase diagram. *Am. Mineral.* **1967**, *52*, 880–885.
13. Eakins, E.; Jayaseelan, D.D.; Lee, W.E. Toward oxidation resistant ZrB<sub>2</sub>-SiC ultra high temperature ceramics. *Metall. Mater. Trans. A* **2011**, *42*, 878–887. [[CrossRef](#)]



© 2015 by the authors; licensee MDPI, Basel, Switzerland. This article is an open access article distributed under the terms and conditions of the Creative Commons Attribution (CC-BY) license (<http://creativecommons.org/licenses/by/4.0/>).